J. Chem. Soc. Nigeria, Vol. 50, No. 4, pp 888 – 908 [2025] https://dx.doi.org/10.4314/jcsn.v50i4.15

POLY(PROPENONITRILE) AS ANTI-CORROSIVE AGENT FOR MILD STEEL IN 0.1M HYDROCHLORIC ACID SOLUTION: EXPERIMENTAL, DFT AND MOLECULAR DYNAMIC SIMULATION STUDIES

U. C. Onyeije,[1] A. I. Obike,[2]* M. C. Egbujor,[3] C,O. Alisa,[4] C. N. Emeruwa,[5] C. Onwuka,[3] and C. Enyia,[4]

[1] Department of Pure and Industrial Chemistry, Nnamdi Azikiwe University, Awka, Nigeria
[2] Department of Pure and Industrial Chemistry, Abia State University, Uturu, Abia State, Nigeria
[3] Department of Chemistry, Federal University Otuoke, Bayelsa State, Nigeria, Aba, Abia State, Nigeria,
[4] Department of Chemistry, Federal University of Technology, Owerri, Nigeria.
[5] Department of Chemical Sciences, Rhema University, Aba

*Corresponding Author' e-mail: ai.obike@abiastateuniversity.edu.ng

ABSTRACT

The anticorrosion studies of poly(propenonitrile) (PPN) on mild steel in acidic media was carried out in 0.1 M HCl using gasometric, gravimetric, and electrochemical techniques at room temperature and at elevated temperatures (303, 313, 323 and 333 K). In all test settings, the inhibitory effectiveness changed in direct proportion to the PPN concentration and in inverse proportion to the exposure duration and temperature. The anticorrosion potential of PPN is attributed to the adsorption of its molecules on the metal surface, blocking the active corrosion sites on mild steel. The adsorption mechanism conformed to the Langmuir and Temkin adsorption isotherm models with the best fits recorded for the Langmuir model (R2 of 0.998). The thermodynamic parameters obtained; Gibbs free energy (ΔGo ads) as well as activation energy (Ea), all favored a spontaneous and exothermic physical adsorption reaction mechanism of PPN. Electrochemical impedance spectroscopy (EIS) obtained revealed increasing charge transfer resistance as PPN concentration increases. The DFT study, shows a significant value for electronegativity in both neutral (3.751 eV) and protonated (2.873 eV) states which indicates that PPN favors strong adsorption. MDs studies corroborated the strong adsorption and further revealed the inhibitor was more stable in its neutral form than in its protonated state, with energy differences of 6.507 eV and 4.961 eV, at 298 ºC and 318 ºC respectively. The results of the several test carried out were all fully connected to one another.

Key words: Poly(propenonitrile), Mild steel, Corrosion inhibition, Gravimetric, Spectroscopy, Polarization, DFT, MDs.

INTRODUCTION

Mild steel, a ferrous metal containing about 0.29% maximum carbon has found wide applications in engineering, industrial and domestic settings [1]. However, its durability is being hampered by corrosion which has become a perennial problem in both developed and developing nations of the world. The estimated cost of corrosion is currently alarming with a negative impact on the global gross domestic product (GDP) [2]. Amongst the numerous forms of iron, mild steel has the advantage of being the cheapest amongst the other alloy steels because it is a readily available raw material and its cost of manufacture is very low [3]. The successful techniques applied in the corrosion inhibition of mild steel in acidic medium are commendable [4-5] and form the basis for this work. Most metals corrode when they are exposed to aggressive media such as humidity, acids, bases, salts, oils, aggressive metals polishes, and liquid chemicals [6-7]. However, the life span of the mild steel in contact with acidic medium depends on the protection or inhibition techniques adopted in such an environment [8].

In view of the fact that the use of chemical inhibitors remains one of the most protective method against

ISSN 0795 - 22066

mild steel corrosion, several inhibitors both synthetic and natural have been reportedly studied and applied to control the rate of corrosion of mild steel and the results obtained have been encouraging [9-12]. However, the toxicity associated with several corrosion inhibitors which contaminates the environment and negatively impact on living things but also poison the environment remains a concern [13-15]. Thus, polymeric inhibitors which are more ecofriendly have increased in importance recently. For instance, PPN has been reported as an effective corrosion inhibitor for certain metals in saline water which is acidic [16]. Amongst the acidic media, hydrochloric acid has been found to be a more effective medium for corrosion evaluation than several acids and its concentration has been found to influence the corrosion rate of mild steel [17-19], this fact has guided our choice of 0.1M HCl medium. Thus this work was designed to investigate the inhibitory activity of PPN (figure 1) as a polymeric inhibitor against the corrosion of mild steel in 0.1M HCl medium via experimental and computational studies.

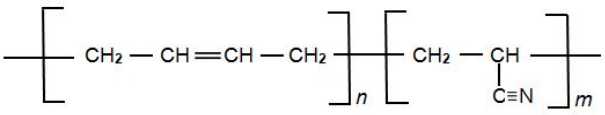

Figure 1: Structure of Poly(propenonitrile) (PPN)

MATERIALS AND METHODS

Materials, Collection and Preparation

The mild steel sample used was procured from Ken Johnson Nigeria Limited, situated in Uyo, Akwa Ibom State, Nigeria. The chemical composition of the mild steel (% wt) were C (0.17 %), Si (0.26 %), Mn (0.46 %), P (0.0047 %), S (0.017 %) and Fe (98.935), In order to obtained coupons for weight loss method, the mild steel sheet was mechanically press cut into coupons, each of dimension, 5 x 4 cm. For electrochemical experiments, the mild steel sheet was cut into coupons of 2 x 1.5 cm dimension. Every coupon was polished with series of emery paper of variable grades starting with the roughest and then the smoothest (600). Ethanol was used to wash and acetone was used to clean thereafter, stored in a desiccator after air drying. The PPN was purchased from Sigma Aldrich. All reagents used were of analytical grade. This included HCl, zinc dust, NaOH, ethanol and acetone.

MATERIALS AND METHODS

Weight loss experiment

In weight loss experiment, a previously weighed mild steel coupon was completely immersed in 250 ml of the test solution (i.e, different concentrations of acid, inhibitors) in a beaker. The beaker was inmersed in a water bath maintained at 30 °C temperature. Similar experiments were repeated at 40, 50 and 60°C. In each case, the weight of the sample before immersion was measured using Scaletec high precision balance (Model, SPB31) after every 24 hours, each sample was withdrawn from the test solution, washed in a solution of NaOH containing aluminum dust and dried in acetone

ISSN 0795 - 22066

before re-weighing. The weight differential for a duration of 168 hours was taken as total weight loss. The inhibition efficiency (%η) for each inhibitor was calculated using the formula,

$$\%I = \left(1 - \frac{W_1}{W_2}\right) \times 100 \quad (1)$$

Where W_1 and W_2 are the weight losses (g/dm^3) for mild steel in the presence and absence of inhibitor in HCL solution, respectively. The degree of surface coverage θ is given by equation 2:

$$\theta = \left(1 - \frac{W_1}{W_2}\right) \quad (2)$$

The rates of corrosion of mild steel in different concentrations of HCl were determined for 168h immersion period from weight loss using Equation 3 [20]

$$Corrosion\ rate\ (mpy) = \frac{W}{At} \quad (3)$$

Where W = weight loss (mg); A = area of specimen (square inches) and t = period of immersion (hour).

Electrochemical methods of measurement

The electrochemical cell used for the study was a cylindrical pyrex vessel, closed with a cap containing five openings. Three of the openings were used for the electrodes. The working electrode was mild steel with surface area of 0.28 cm^2 in 2 M solution of HCl. A saturated calomel electrode (SCE) was used as a reference electrode. The counter electrode was a platinum plate of surface area, 1 cm^2.

Electrochemical impedance spectroscopy measurement

The electrochemical impedance spectroscopy (EIS) measurements were conducted using a frequency range of 10 to 100,000 Hz at 303 Kelvin, with a 5mV RMS peak-to-peak AC signal amplitude, at open circuit potential and in air. Nyquist plots and the polarization resistance R_p, was used to obtain the impedance date via diameters of the semi-circle in the Nyquist plot. The R_p included charge transfer resistant (R_{ct}), diffuse layer resistance (R_d), the accumulated species resistance at the metal/solution interface (R_a) and the resistance of the film (in the presence of the inhibitor) at the metal surface (R_f). The polarization potential (R_p) was calculated using Equation 4.

$$R_p = R_{ct} + R_d + R_a + R_f \quad (4)$$

From the impedance spectroscopy data, the inhibition efficiency was calculated using the following equation,

$$\%IE = \frac{R_p^{inh} - R_p^o}{R_p^{inh}} \times \frac{100}{1} \quad (5)$$

The double layer capacitance (C_{dl}) was calculated using Equation 3.7

$$C_{dl} = \frac{1}{2\pi R_p f_{max}} \quad (6)$$

Where f_{max} is the maximum frequency the Nyquist plot (hour).

Effect of temperature measurement

The effect of temperature on the corrosion of mild steel in solution of HCl in the absence and presence of PPN was investigated using the Arrhenius equation, which can be written as follows,

$$CR = Aexp\left(\frac{-E_a}{RT}\right) \quad (8)$$

ISSN 0795 - 22066

Where CR is the corrosion rate of mild steel in solution of HCl, A is the Arrhenius constant, Ea is the minimum energy required before adsorption of the inhibitor can occur, R is the universal gas constant and T is the temperature. From the logarithm of equation 8, equation 9 was obtained,

$$logCR = logA - \frac{E_q}{2.303RT} \quad 9$$

From equation 9, a plot of logCR versus 1/T an expression that is "linear with slope and intercept equal to Ea/R and logA respectively.

Adsorption and Thermodynamic examination

The Transition state equation was used to obtain Thermodynamic parameters for the adsorption of PPN on mild steel surface as shown below,

$$CR = \frac{RT}{Nh} exp\left(\frac{\Delta S^0_{ads}}{R}\right) exp\left(\frac{-\Delta H^0_{ads}}{RT}\right) \quad 10$$

Where Avogadro's number is N, Plank constant is h, standard entropy of adsorption is ΔS^0_{ads} and the standard enthalpy of adsorption is ΔH^0_{ads}

$$ln\left(\frac{CR}{T}\right) = ln\left(\frac{R}{Nh}\right) + \frac{\Delta S^0_{ads}}{R} - \frac{\Delta H^0_{ads}}{RT} \quad 11$$

That a plot of $ln\left(\frac{CR}{T}\right)$ versus 1/T should give a straight line with slope and intercept equal to $\frac{\Delta H^0_{ads}}{R}$ and $(ln\left(\frac{R}{Nh}\right) + \frac{\Delta S^0_{ads}}{R})$, respectfully.

Adsorption models

Different adsorption isotherm models (Langmuir, Temkin, Flory-Huggins, Frumkin, El awardy and Freundlich) were used to investigate the adsorption behavior of the inhibitors by fitting the data obtained for degree of surface coverage into different equations. The assumptions establishing the Langmuir adsorption model can be written as,

$$log\left(\frac{C}{\theta}\right) = logk_{ads} - logC \quad 12$$

Where k_{ads} is the adsorption equilibrium constant and θ is the degree of surface coverage of the inhibitor. From equation 12, a plot of $log\left(\frac{C}{\theta}\right)$ versus logC is a straight line with slope and intercept equal to unity and $logk_{ads}$ respectively.

DFT and MDS Study

Applying the Koopmans theorem, the frontier molecular orbitals that is the HOMO (Highest occupied molecular orbital) and the LUMO (Lowest unoccupied molecular orbital) were investigated. The global reactivity parameters which include; Chemical hardness (η), Chemical potential (μ), Chemical softness (*S*), Electrophilicity (ω), and Electronegativity (χ) were evaluated using the HOMO, LUMO data and computed using equations 13-18.

$$Eg = E_{HOMO} - E_{LUMO} \quad 13$$

$$\mu = \frac{IP+EA}{2} \quad 14$$

$$\sigma = \frac{I}{2\eta} \quad 15$$

$$\eta = \frac{IP-EA}{2} \quad 16$$

$$\chi = -\mu = \frac{IP+EA}{2} \quad 17$$

$$\omega = \frac{\mu^2}{2\eta} \quad 18$$

The stabilization energy of the investigated compound for the most interacting donor and acceptor orbitals was computed with equation 19.

$$E^{(2)} = \Delta E_{i,j} = -q_i \frac{F^2(i,j)}{\varepsilon_i - \varepsilon_j} \quad 19$$

ISSN 0795 - 22066

Where q_i depicts the donor orbital occupancy, ε_i and ε_j are the diagonal elements and $F_{(i,j)}$ is the Fock matrix element.

However, survey of literature shows that, to obtain the most desirable and captivating adsorption configuration of the inhibitor investigated, molecular dynamic modeling is better evaluated. The first phase in this computer research is the geometry optimization (i.e., energy minimization) of the corrosion inhibitor investigated. which is a part of so many phases involved in modeling approach. To maximize the inhibitors analysed and their interactions, A'smart' method was used, which started with the steepest descent path, then followed the conjugate gradient path, and finally completed with the Newton's approach [21-23]. After maximizing the form of the inhibitor of interest, the simulation box was generated using the mild steel surface. Dynamic simulations were also observed. Equation 20 was used to ascertain the interactivity on approaching equilibrium and the adsorption energy of PPN on the mild steel surface. The binding energy, also known as MD energy, was determined

$$E_{ads} = E_{total} - (E_{metal\ surface} + E_{inhibitor}) \quad 20$$

Where, E_{total}, $E_{metal\ surface}$, $E_{inhibitor}$ represents the energies of inhibitor/mild steel surface, mild steel surface and inhibitor PPN respectively.

RESULTS AND DISCUSSION

Weight loss

Results obtained for weight loss variation with time for the corrosion of mild steel in 0.1 M HCl with different concentrations of PPN at 303, 313, 323 and 333 K are represented in figures 2, 3, 4 and 5 respectively. The figures revealed that corrosion of mild steel in the absence of PPN (blank) showed marked difference from those obtained in its presence, suggesting that there is a higher corrosion rate in the absence of PPN than in the presence of PPN. The figures also reveal that the downward arrangement of the plots as concentration of PPN increases indicate that inhibition of corrosion by PPN was dependent on concentration and it increased as concentration of the inhibitor increased. Positive correlation with temperature was observed in the plots shown in Figures 2 to 5. This means that as temperature increased corrosion rate increased.

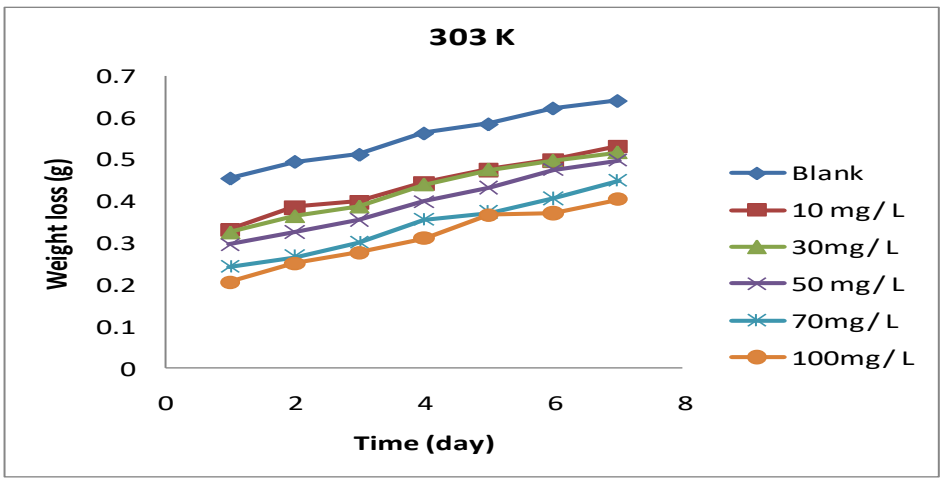

Fig. 2: Variation of weight loss with time for the corrosion of mild steel in 0.1 M HCl in the absence and presence of various concentrations of PPN at 303 K.

ISSN 0795 - 22066

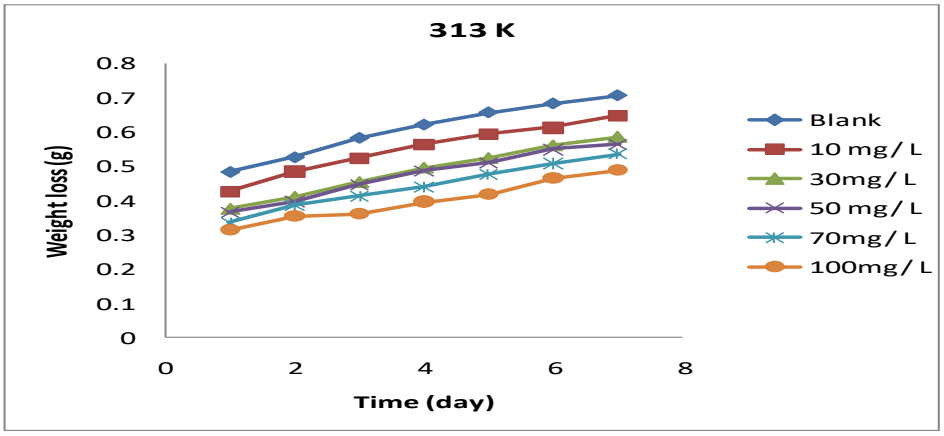

Fig. 3: Variation of weight loss with time for the corrosion of mild steel in 0.1 M HCl in the absence and presence of various concentrations of PPN at 313 K

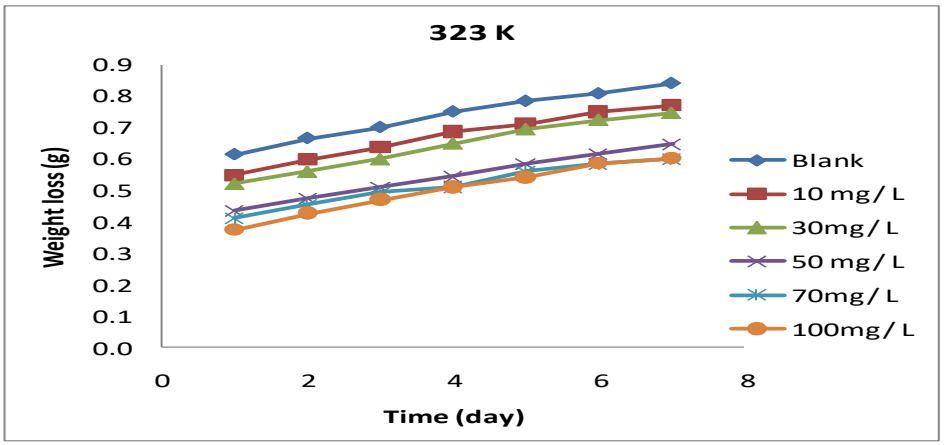

Fig. 4: Variation of weight loss with time for the corrosion of mild steel in 0.1 M HCl in the absence and presence of various concentrations of PPN at 323 K

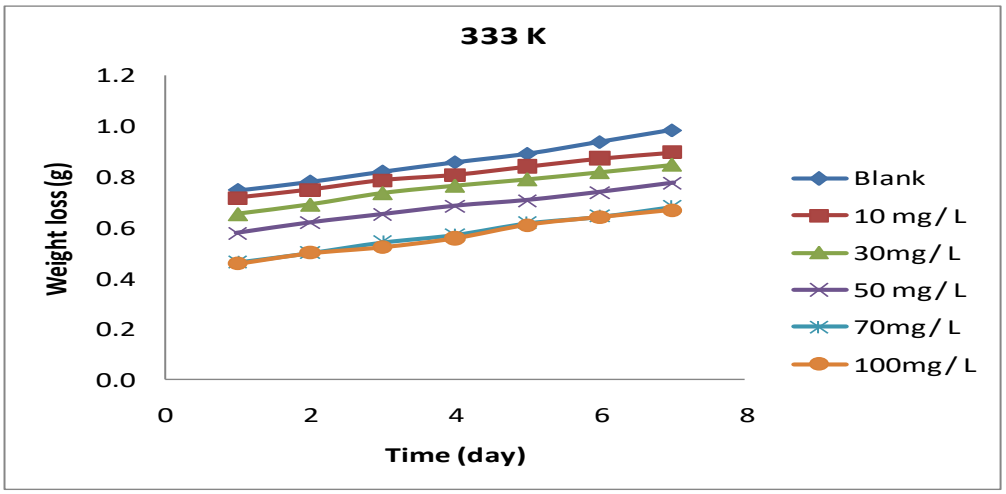

Fig. 5: Variation of weight loss with time for the corrosion of mild steel in 0.1 M HCl in the absence and presence of various concentrations of PPN at 333 K.

ISSN 0795 - 22066

Table 1: Inhibition efficiency and degree of PPN for the corrosion of mild steel in 0.1 M HCl

C (mg/L)	303 K	333 K	303 K	333 K
10	36.82	32.19	19.68	8.92
30	38.60	23.04	27.48	14.00
50	40.86	35.04	30.20	21.20
70	46.67	40.62	33.66	30.73
100	52.02	42.04	39.48	32.15

From the above analysis, it can be stated that the corrosion of mild steel in solutions of HCl followed kinetic principles which expect the rates of all chemical reactions to increase with increase in temperature and with the period until all the reactant have reacted. The effects of PPN on the corrosion of mild steel in solutions of HCl clearly point toward inhibition. Therefore, PPN inhibited the corrosion of mild steel in solutions of HCl. Consequently, since the extent of inhibition depends on temperature and concentration of PPN, then it can be stated that the inhibition efficiencies of PPN for the corrosion of mild steel in solutions of HCl depended on the concentration of inhibitor and on temperature of the corroding system. In view of this, values of corrosion rate of mild steel and inhibition efficiencies of PPN (calculated from equation 1) is presented in Table 1. The corrosion rates of mild steel in solutions of HCl were seen to increase with the period of contact and with increasing temperature but decreased with increase in the concentrations of the inhibitors. On the other hand, the inhibition efficiency increased with increase in the concentration of the inhibitors but decreased with increasing temperature. This suggests that the mechanism of inhibition of corrosion by PPN was by physical adsorption on the surface of mild steel. It has been reported that for a physiosorption mechanism, the extent of adsorption (as measured by inhibition efficiency) decreases with increase in temperature, whereas for chemical adsorption, the extent of adsorption decreases with increase in temperature [24]. The increase in inhibition efficiency with increasing concentration indicated that the extent of adsorption increased as the concentration of the inhibitor was increased. This is possible because with increasing inhibitor concentration, the fraction of the inhibitor transported to the surface of the mild steel would normally increase correspondingly. In summary, the figures (2-5) generally reveal that the corrosion of mild steel in solutions of HCl is dependent on (i) period of immersion (ii) temperature and (iii) concentration of PPN

Electrochemical method

Electrochemical impedance spectroscopy (EIS)

The electrochemical impedance data for corrosion of mild steel in 0.1 M HCl in the absence and presence of PPN is presented in Table 2. The observed electrochemical impedance (R) in the absence of PPN was 58.24 Ωcm^2. However, the electrochemical impedance (R) increased in the presence of PPN with increase in concentration. The corrosion rate was dependent on electrochemical efficiency and inhibition efficiency. This corroborates the dependency of corrosion rate and inhibition efficiency on the concentration of inhibitor observed in the weight loss experiments discussed in section 3.1.

ISSN 0795 - 22066

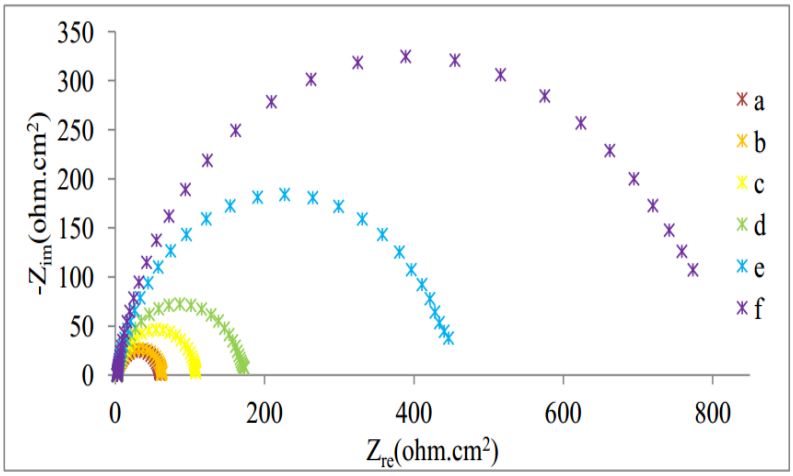

Fig. 6: Nyquist plot for mild steel in 0.1 M HCl in the absence and presence of various concentrations of PPN at 303 K (a= blank, b = 100 mg/L, b = 70 mg/L, c = 50 mg/L, d= 30 mg/L and f = 10 mg/L)

Table 2: Electrochemical impedance parameters for the corrosion of mild steel in the presence of various concentrations of PPN

C (mg/L)	N	Rct (Ωcm2)	%IE
Blank	0.88	58.24	-
10	0.87	264.22	77.96
30	0.86	294.42	80.22
50	0.86	340.24	82.88
70	0.85	385.70	84.90
100	0.83	406.30	85.67

The Nyquist plots for PPN is shown in Fig. 6. The results obtained indicated that the size of the semicircle increases with increasing concentration of the inhibitor which indicates that the inhibition efficiency of the inhibitor increase with increasing concentration. Generally, the wider the semi-circle, the better the inhibition efficiency. The trend of increase in the diameter of the semicircle also reveals that the higher the concentration of the inhibitor, the more the increase, which also confirm that PPN is an adsorption inhibitor for mild steel in solution of HCl. It is significant that the Nyquist plots in Fig.6 does not display perfect semicircle. This frequency dispersion can be attributed to surface heterogeneity connected with structural or interfacial changes arising from impurities or dislocations, fractal structures, distribution of activity centers, adsorption of inhibitors, and formation of porous layers [24, 25].

In the evaluation of Nyquist plots, the difference in real impedance at lower and higher frequencies is commonly considered as a charge transfer resistance. The value of charge transfer resistance indicates the electron transfer across the interface. The CPE is used instead of double layer capacitance, C_{dl} in the equivalent circuit in order to fit the data more accurately. The introduction of such a CPE is often used to interpret data for the rough solid

ISSN 0795 - 22066

electrodes. Also, there is a parameter obtained to measure the non-ideality of the capacitor which is known as surface irregularity, n which has a value range of $0 < n < 1$. The decrease of n values in the presence of PPN could be explained by increment in surface heterogeneity, probably due to the heterogeneous distribution of adsorption of the inhibitors on the active sides.

Effect of temperature study

The Arrhenius plots for the corrosion of mild steel in solution of HCl in the presence of various concentrations of PPN are presented in Fig. 9. Values of Arrhenius constant deduced from the plots are presented in Tables 5. The plots generated values of R^2 that are very close to unity, which confirm that the present data fit Arrhenius model. The results presented in Table 5, showed that the activation energies ranged from 5.42 to 13.17 J/mol for PPN. These are within the range (<80 kJ/mol) of values expected for the mechanism of physical adsorption. Therefore, the adsorption of PPN on the surface of mild steel is consistent with the mechanism of charge transfer from charged inhibitor to charged metal surface. Generally, E_a values were very low, which indicate that diffusion of the inhibitor molecule to the surface of the mild steel might have contributed to the rate of adsorption of the inhibitors' molecules to the surface of the mild steel. The activation energy for the blank (5.42 J/mol) was lower than those calculated for the inhibited system indicating that the corrosion of mild steel was retarded by PPN. It is also significant to state that values of activation energy obtained for PPN were high, which justify the fact that PPN is a good inhibitor for mild steel in 0.1 M HCl.

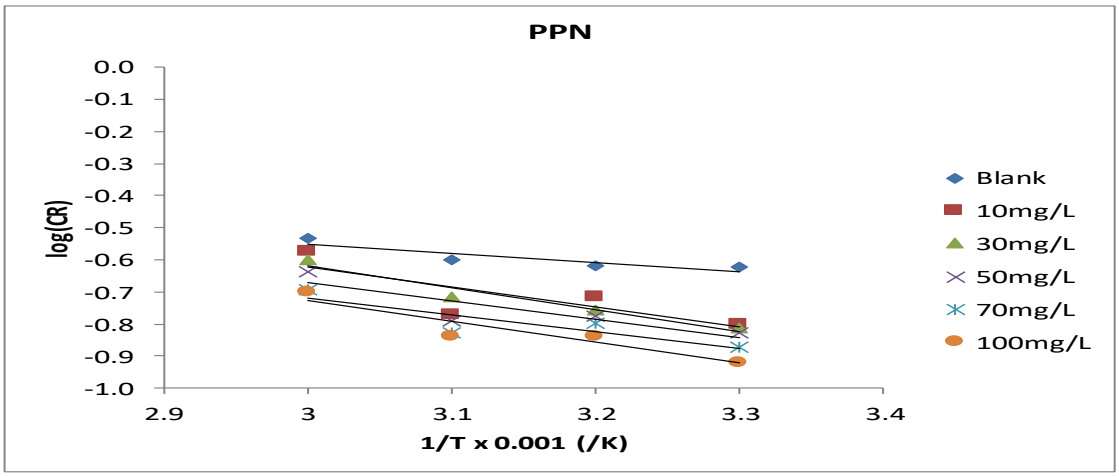

Fig. 9: Arrhenius plot for the corrosion of mild steel in 0.1 M HCl in the absence and presence of various concentrations of PPN

ISSN 0795 - 22066

Table 5: Activation parameters for the corrosion of mild steel in solution of HCl containing various concentrations of PPN

C (mg/L)	Slope	logA	Ea (J/mol)	A	R2
Blank	0.283	0.299	5.42	1.99	0.774
10	0.626	1.259	11.99	18.16	0.644
30	0.688	1.447	13.17	28.01	0.947
50	0.566	1.026	10.84	10.62	0.757
70	0.516	0.828	9.88	6.73	0.744
100	0.656	1.243	12.56	17.51	0.871

Thermodynamic/adsorption considerations

The Transition state plot for the corrosion of mild steel in solutions of HCl, containing various concentrations of PPN is presented in Fig. 10. Transition state parameters derived from the plots are presented in Table 6. The plots displayed high degree of linearity as measured by the values of R^2, which were close to unity. Values of the standard enthalpy of adsorption were seen to be negative, indicating that the adsorption of the inhibitors was exothermic. On the other hand, entropy values were positive, pointing toward increasing disorderliness.

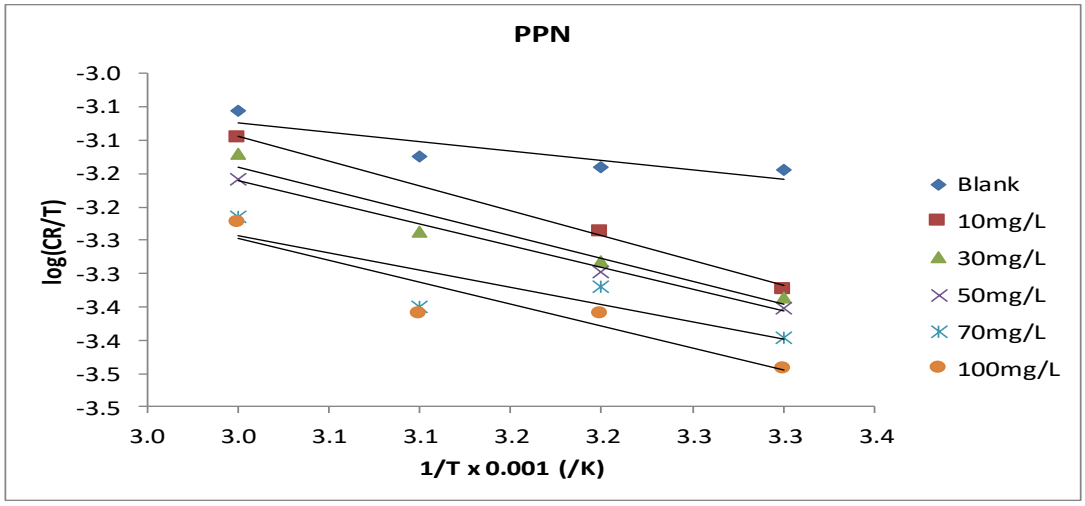

Fig. 10: The Transition state plot for the corrosion of mild steel in solution of HCl in the absence and presence of various concentrations of PPN

ISSN 0795 - 22066

Table 6: Transition state parameters for the adsorption of PPN on mild steel surface

C (mg/L)	Slope	Intercept	ΔH^0_{ads} (J/mole)	ΔS^0_{ads} (J/mol)	R2
Blank	0.283	-2.223	-2.35	70.31	0.7740
10	0.750	-0.842	-6.24	81.79	0.9970
30	0.688	-1.075	-5.72	79.86	0.9470
50	0.651	-1.206	-5.41	78.77	0.9960
70	0.516	-1.693	-4.29	74.72	0.7440
100	0.656	-1.279	-5.45	78.16	0.8710

Adsorption Models

The tests revealed that Langmuir and Temkin adsorption isotherms best fitted the adsorption of PPN on the surface of mild steel. The Langmuir isotherms for the adsorption of PPN on the surface of mild steel is represented in Fig 11. Adsorption parameters deduced from the plots is presented in Table 7. The results obtained indicated that the plots displayed high values of R^2 which agrees with the linearity of the equation. However, the slopes were less than the ideal value of unity, indicating that there was interaction between adsorbed species.

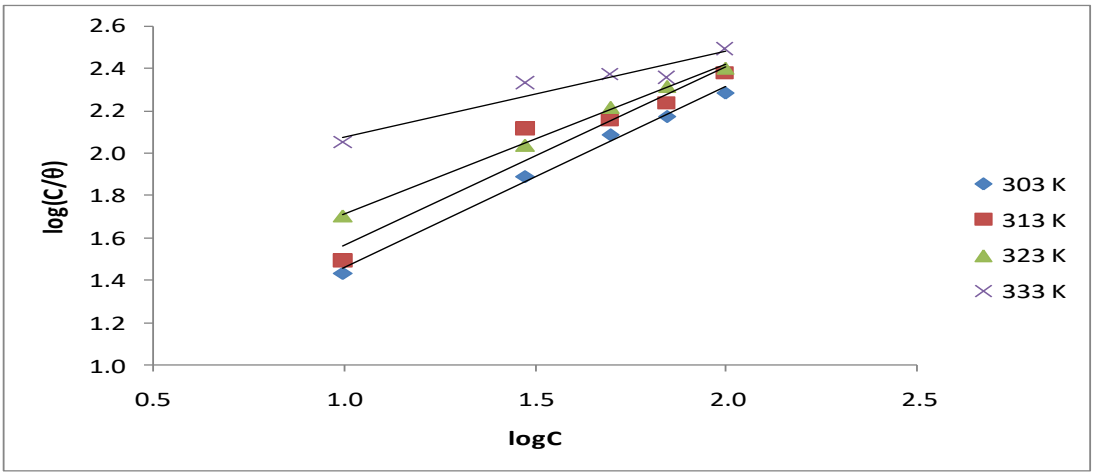

Fig. 11: Langmuir isotherm for the adsorption of PPN on mild steel surface

To compensate for the existence of interaction (as revealed by the non-unity of values for slope obtained in the Langmuir adsorption model), other isotherms were considered, and it was found that Temkin isotherm best described the deviation. The Temkin adsorption isotherm can be written as follows

$$\theta = \frac{-\ln k_{ads}}{2a} - \frac{\ln C}{2a} \qquad 21$$

From equation 21, a plot of θ versus logC should give a straight line with slope equals to 2.303 x a/2

ISSN 0795 - 22066

and intercept equals to 2.303alogk_{ads}/2 provided assumptions of Temkin isotherm are valid. Temkin plots for the inhibition of the corrosion of mild steel in solutions of HCl by PPN is presented in Fig. 12 while Temkin parameters obtained from the plot is presented in Table 8. The results obtained indicated that the data strongly obey the Temkin adsorption model as shown by excellent values of R^2. The interaction parameters are all positive, indicating the attractive behavior of the inhibitors. The equilibrium constant of adsorption (k_{ads}) is related to the standard free energy change of adsorption according to the following equation,

$$\Delta G^0_{ads} = -2.303RTlog(55.5k_{ads}) \quad 22$$

Where ΔG^0_{ads} is the standard free energy change of adsorption, R is the gas constant, T is the temperature and k_{ads} is the equilibrium constant of adsorption. Values of free energy change calculated from k_{ads} values obtained from Langmuir and Temkin isotherms were recorded in Table 8. The results generally revealed that the free energies were negatively less than – 20 kJ/mol. Therefore, the adsorption of PPN on the surface of mild steel was spontaneous and is consistent with the mechanism of physical adsorption

Table 7: Langmuir parameters for the adsorption of PPN on mild steel surface

T (K)	slope	Intercept	ΔG^0_{ads} (J/mol)	R2
303	0.588	0.597	-13.58	0.993
313	0.847	0.715	-14.74	0.936
323	0.71	0.996	-16.95	0.998
333	0.404	1.672	-21.78	0.92

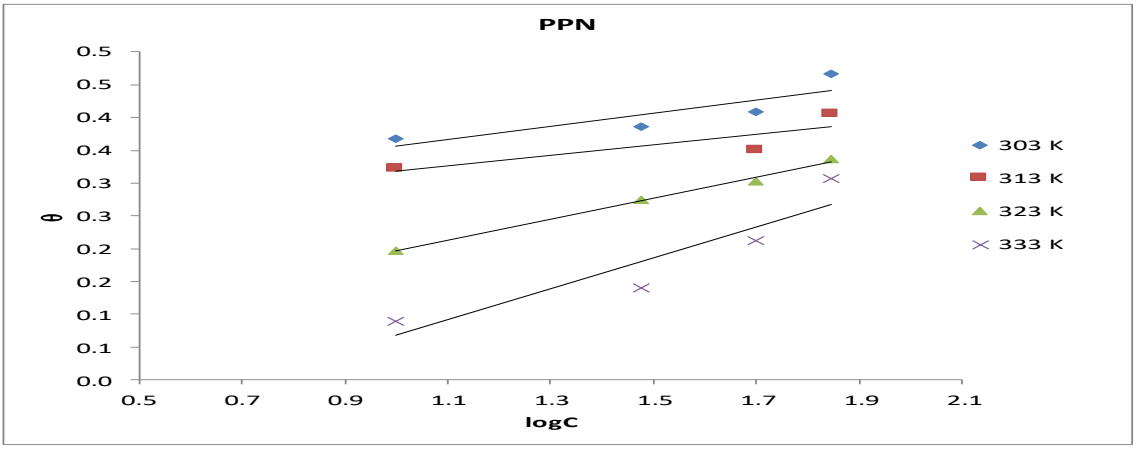

Fig. 12: Temkin isotherm for the adsorption of PPN on the surface of mild steel

ISSN 0795 - 22066

Table 8: Temkin parameters for adsorption of PPN on mild steel surface

T (K)	Slope	intercept	a	logkads	ΔG^0_{ads} (J/mol)	R2
303	0.099	0.257	5.05	0.0254	-10.27	0.737
313	0.081	0.236	6.17	0.0191	-10.57	0.73
323	0.16	0.035	3.13	0.0056	-10.82	0.993
333	0.235	-0.167	2.13	-0.0392	-10.87	0.846

DFT Evaluation

The HOMO, LUMO, Energy gap and quantum descriptors for PPN are represented in table 9.The ionization potential (IP) and electron affinity (EA) are equal to the E_{HOMO} and E_{LUMO}. These orbitals are encompassed with the tendency to donate and accept electrons [26]. The energy gap, which is the difference in energy between the E_{HOMO} and E_{LUMO}, determines the chemical reactivity and stability of the PPN molecule under investigation. [27]. From previous literature, good corrosion inhibitors have low energy gap values and offer electrons to unoccupied orbital and accept free electrons [28]. A high energy gap is associated with stable inhibitors whereas a low energy gap is linked to reactive inhibitor molecules [29]. It is notable that the HOMO, LUMO values, and quantum descriptors were calculated in the protonated (PPN_P also known as CHAB_P) and neutral state (PPN_N also known as CHAB_N) at the B3LYP GD3BJ/6-311++G (d,p) level of theory. See figure 13. for the isosurface of the HOMO, and LUMO orbital distributions. From our result, the higher E_{HOMO} in the neutral state -7.005 eV, and the lower E_{LUMO} -0.498 eV show an electron-accepting capacity of the PPN molecule. On protonation, it is observed that E_{HOMO} reduced from -7.005 eV to -5.354 eV respectively. Also, the E_{LUMO} is found at -0.393 eV, this implies that in both states the PPN molecule is observed with an electron-accepting capacity, but intense in the neutral state [30]. For the energy gap of the molecule, in the neutral state, an Eg of 6.507 eV is found and 4.961 eV is obtained on protonation. Hence, the PPN molecule is more reactive and less stable on protonation and more stable and less reactive in the neutral state. A small value for chemical softness shows that the PPN molecule acts as a soft base [31]. An inhibitor molecule showing higher values of electronegativity will show a stronger ability to interact with the substrate and the PPN molecule shows a significant value for electronegativity in both states, PPN_N (3.751 eV) and PPN_P (2.873 eV) and indicates that PPN molecule favor strong adsorption.

ISSN 0795 - 22066

Table 9. Calculated HOMO, LUMO, Energy gap and quantum descriptors for PPN

Compound	HOMO (eV)	LUMO (eV)	Eg eV	η (eV)	***S*** (eV-1)	μ (eV)	χ (eV)	ω (eV)
PPN_N (CHAB_N)	-7.005	-0.498	6.507	3.253	0.153	-3.751	3.751	2.162
PPN_P (CHAB_P)	-5.354	-0.393	4.961	2.480	0.201	-2.873	2.873	1.632

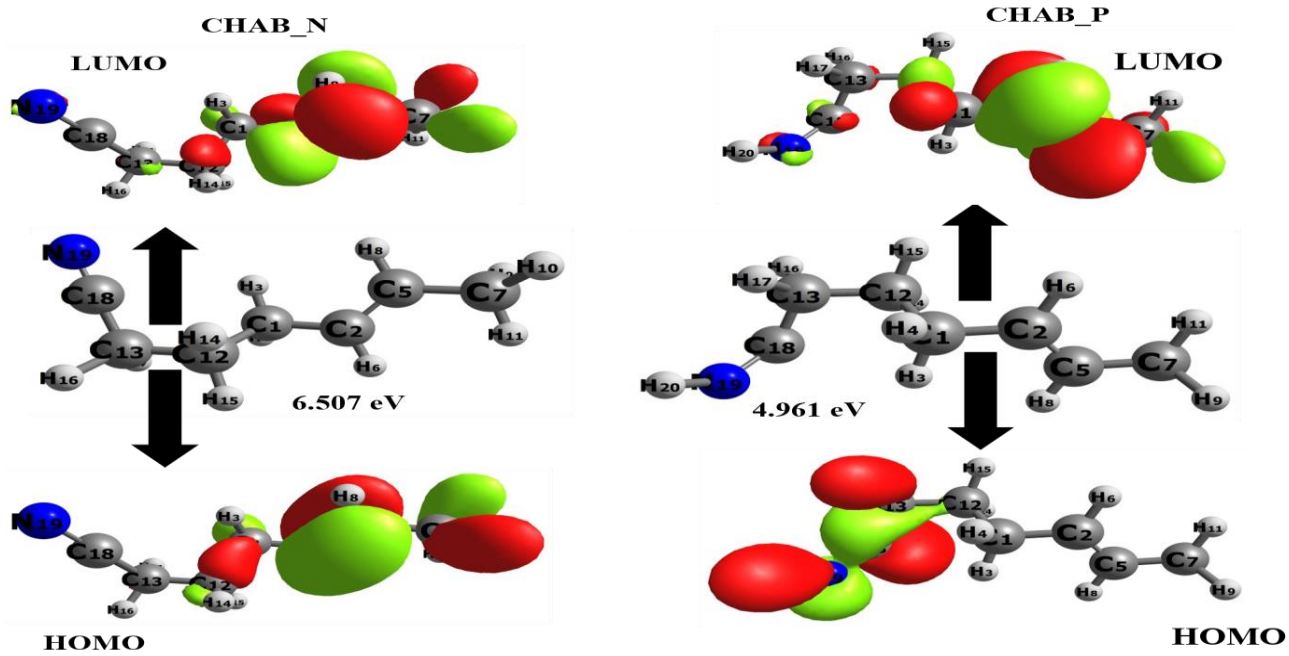

Figure 13. HOMO, LUMO plots for studied compounds showing their respective energy gap

Additionally, the natural bond orbital (NBO) analysis is used to describe the electronic structure of molecules based on the premise that the electron distribution of a molecule can be described using localized molecular orbitals [32]. They provide insight into the nature of the bonding and the stability of the molecule. It is also used to describe the chemical bonds between atoms in a molecule [33]. The NBO analysis explains the interaction between the donor and acceptor orbital with the aid of the second-order perturbation energies which explains the strength of the interacting orbitals. A high E^2 value infers strong intermolecular interaction between the donor and acceptor orbitals. Stabilization energy $E^{(2)}$ of the most interacting donor and acceptor orbitals of the studied compounds is displayed in table 10. From the result, it can be seen that the most dominant type of interaction is that of non-bonding interaction and anti-bonding interaction. In the neutral state, transition between LP- σ*, σ- σ*, σ- π* and π- σ* were observed with corresponding stabilization energies 10.00 kcal/mol, 5.11 kcal/mol, 3.95 kcal/mol, 3.39 kcal/mol, and 3.12 kcal/mol

ISSN 0795 - 22066

respectively. For the protonated state, the transition between; σ- σ*, σ- σ*, σ- σ*, σ- σ* and σ- σ* produced agreeing stabilization energies of; 3.38 kcal/mol, 3.21 kcal/mol, 2.55 kcal/mol, 2.42 kcal/mol and 1.95 kcal/mol respectively. Herein, based on stabilization energies a strong donor and acceptor interaction is found in the neutral state of the PPN molecule and entails stability, which is consistent with the FMO results.

Table 10. Perturbation energies for the most interacting donor-acceptor orbitals for PPN

Compound	Donor (i)	Acceptor (j)	E2 kcal/mol	E(j)-E(i) a.u	F(I,j) a.u
PPN_N (CHAB_N)	LP N19	σ*C13-C18	10.00	0.84	0.082
	σC5-H8	σ*C2-H6	5.11	0.99	0.064
	σC7-H10	π*C2-C5	3.95	0.55	0.042
	πC2-C5	σ*C1-H4	3.39	0.69	0.043
	πC2-C5	σ*C7-H10	3.12	0.70	0.042
PPN_P (CHAB_P)	σN19-H20	σ*C18-N19	3.38	1.73	0.097
	σC13-C18	σ*C18-N19	3.21	1.63	0.091
	σC5-H8	σ*C2-H6	2.55	0.99	0.064
	σC13-H17	σ*C13-N19	2.42	0.62	0.049
	σC1-C2	σC5-C7	1.95	0.98	0.055

Furthermore, the molecular electrostatic potential (MESP) is known to provide more insight into a molecule's polarity and hydrogen bonding. Similarly, it is an essential tool in studying the reactivity of molecules and their affinity toward positively or negatively charged molecules [34]. MESP explains the charge distribution within the different chemically active regions (sites) of the molecules (electrophilic and nucleophilic sites), which presents a detailed explanation of the intermolecular interactions for the studied compound [35]. Utilizing the GaussView 0.6 [36], the colored map of the MESP showing the region of nucleophilic and electrophilic attack is presented in figure 14. The created surface map for MESP contains three colors, which are explained using a color scale. the blue color indicates positive charge which is areas that are low on electrostatic potential density (electron-poor areas), the yellow areas consist of negative charges that are to say it has a high electrostatic potential density (electron-rich areas), and the green color indicates mean potential [37]. Herein, the presence of different colors suggests that excessive charge separation takes place in all studied compounds. Also, the electron-poor areas are found on the N atom for both the neutral and protonated states of the studied molecule. On protonation, the blue colors become dense on the N atom. The positive (blue) regions are located on hydrogen atoms which are related to nucleophilic reactivity (strongest attraction) which are found on the entire PPN molecule. The color code of these maps is in the range between -7.264 a.u (green) and -7.264 a.u (blue). Due to this molecule reactive sites activity, PPN can serve as an inhibitor molecule.

ISSN 0795 - 22066

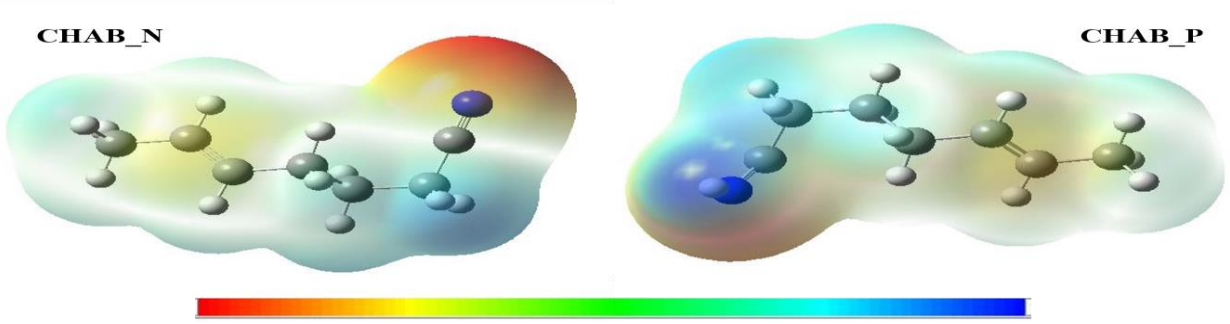

Figure 14. Colored MESP Map for studied PPN

Molecular dynamic simulation (MDS)

Molecular dynamic simulation (MDS) was used in this study to further assess the adsorption and mechanistic properties of the studied inhibitor on the relevant metallic surfaces [38, 39]. It is possible to activate and evaluate the interaction behaviour of the investigated inhibitors on the surface of mild steel using (MDS) analysis. The binding energy, also known as MD energy was determined as shown in Table 11. Table 11 summarizes the observed interaction and simulation energies, and Figure 3 depicts the top and side adorable adsorption configurations of the investigated inhibitor molecule PPN on the mild steel surface for graphical evaluation and stability checks. Figure 15 shows that PPN adsorbs on the mild steel surface in essentially parallel or flat configurations. This is due to the establishment of a strong coordinating connection and a back bond between the inhibitor molecule and the Fe-atom of the metal surface. Literature review shows that the larger the surface coverage of the inhibitor, the better the inhibitor's inhibitory efficacy. The inhibitor PPN in this study adsorb in the flat orientation. The results presented herein showed the inhibition effectiveness of PPN to be -2.913183 kcal/mol at its neutral state and -7.698017 for the protonated system respectively. Temperature effect was also evaluated in this concept using different temperatures in the molecular dynamic simulation analysis, were 298 ºC and 318 ºC respectively were utilized during molecular dynamic simulation. The adsorption energy of PPN on the mild steel surface was calculated according to Equation 20.

The adsorption of the studied inhibitor (PPN) on the mild steel surface gave the computed values of interaction energy as thus: -78.4152 kcal/mol and -77.2332 for 289 ºC, and 318 ºC, respectively for the neutral inhibitors. Also, for the protonated system, the adsorption energy was observed to be -77.2890 kcal/mol and -76.2890 kcal/mol for the studied temperature 289 ºC, and 318 ºC accordingly. This interaction was shown to be consistent with the analysis of the frontier molecular orbital analysis, since the inhibitor was more stable in its neutral form than in its protonated state, with energy differences of 6.507 eV and 4.961 eV, respectively. These greater negative values of interaction energy can be ascribed to the strong contact between the investigated inhibitors molecules and Fe surfaces. It

ISSN 0795 - 22066

is important to note that the smaller energy gap which indicated higher chemical reactivity resurfaced in the adsorption behavior of this inhibitor (PPN) on the mild steel surface. This demonstrates the system's capacity to guard against corrosion. Similarly, it was discovered that increasing the temperature reduced the interaction energy of the examined system.

Table 11: Interaction and simulation energies of the studied inhibitors PPN_N (CHAB_N) and PPN_P (CHAB_P) at 298 k and 318 k on mild steel surface

nhibitor (PPN)	Inhibitor energy (Kcal/mol)	Temperature (k)	MD Simulation energy	Interaction energy
Neutral	-2.913183	298	-75.502	-78.4152
Protonated	-7.698017	298	-69.591	-77.2890
Neutral	-2.913183	318	-74.320	-77.2332
Protonated	-7.698017	318	-68.591	-76.2890

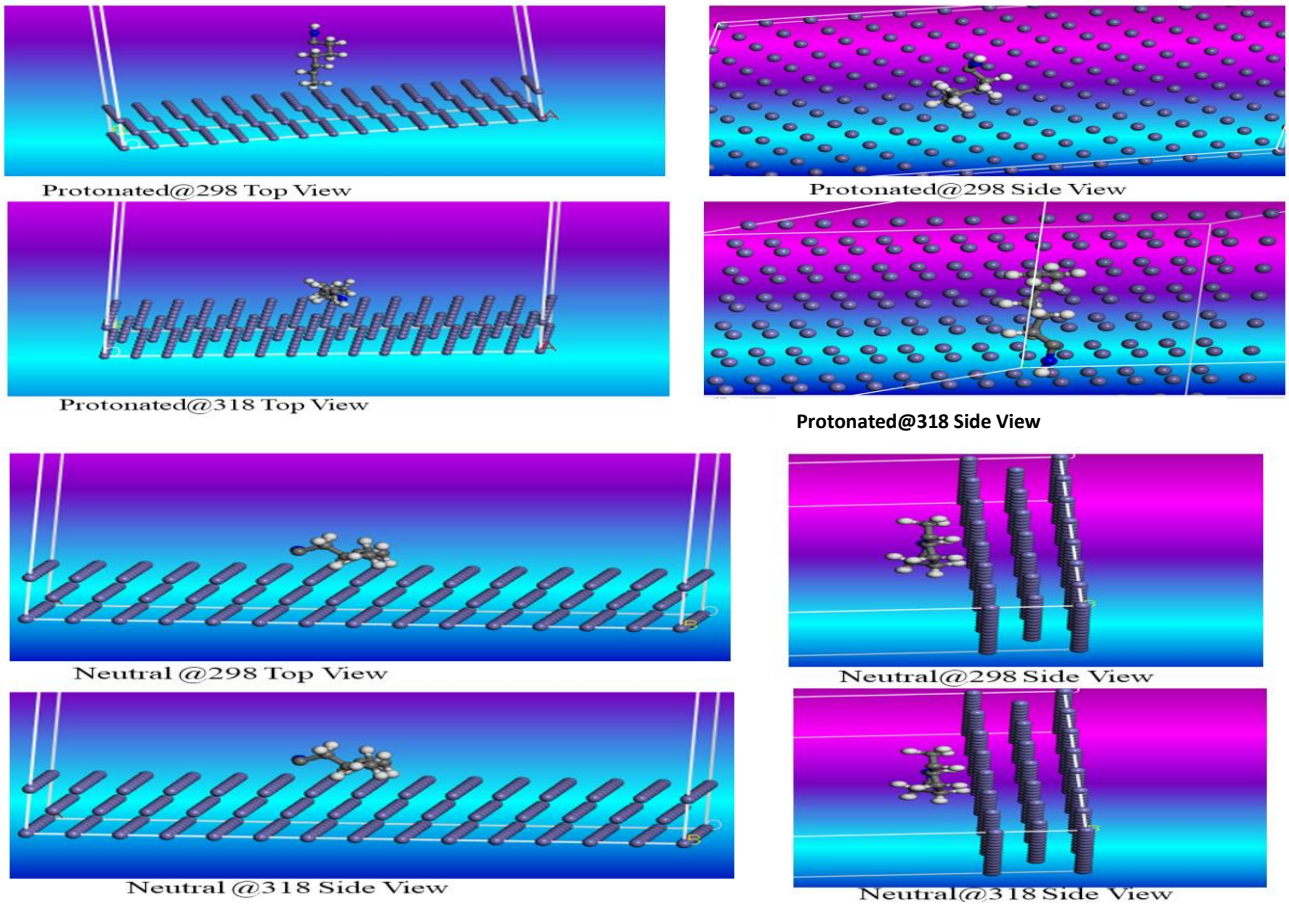

Figure 15: Top and Side view of the interaction between the studied inhibitor (PPN) with the mild steel surface at 298 K and 318 K

ISSN 0795 - 22066

CONCLUSION

This study sought to examine, the corrosion inhibition properties of PPN for mild steel in solutions of HCl. The results obtained from all the analytical techniques generally revealed that PPN inhibited the corrosion of mild steel in solutions of HCl and that the inhibition efficiency PPN increased with increase in concentration but decreased with increasing temperature. Kinetic and thermodynamic investigations indicated that the range of values obtained for the activation energy are in agreement with the mechanism of physical adsorption, which implies that the inhibitors function best at lower temperature. These findings confirm the trend obtained for the variation of inhibition efficiency with temperature. Electrochemical data revealed the dependence of increase in inhibition rate on PPN concentration. Thermodynamic feasibility study revealed that the adsorption of the inhibitor was spontaneous, exothermic and consistent with the mechanism of physical adsorption. The electronegativity values indicate that PPN molecule favor strong adsorption. The reactive sites activity and adsorption behavior of PPN on the mild steel surface indicate that PPN can serve as an effective anti-corrosive agent for mild steel.

REFERENCES

1. A.J. Mwakalesi, Corrosion inhibition of mild steel in sulphuric acid solution with *tetradenia riparia* leaves aqueous extract: kinetics and thermodynamics, *Biointerface Res Appl Chem*., 2023, 13, no. 1, 32. doi: 10.33263/BRIAC131.032.

2. B. Wei and J. Xu, Special Issue: Environmental corrosion of metals and its prevention: an overview and introduction to the special issue, *Coatings*, 2022, 12, no. 7, 1013. doi: 10.3390/coatings12071013.

3. K. Muthamma, P. Kumari, M. Lavanya and S.A. Rao, Corrosion inhibition of mild steel in acidic media by *N*-[(3,4-dimethoxyphenyl)methyleneamino] -4-hydroxy-benzamide, *J Bio Tribo Corros*., 2021, 7, no. 1, 10. doi: 10.1007/s40735-020-00439-7.

4. B.S. Mahdi, M.K. Abbass, M.K. Mohsin, W.K. Al-azzawi, M.M. Hanoon, M.H.H.Al-kaabi, L.M. Shaker, A.A. Al-amiery, W.N.R.W.Isahak, A.A.H. Kadhum and M.S. Takriff, Corrosion inhibition of mild steel in hydrochloric acid environment using terephthaldehyde based on schiff base: gravimetric, thermodynamic, and computational studies, *Molecules*, 2022, 27, no. 15, 4857. doi: 10.3390/molecules27154857.

5. I.A. Annon, A.S. Abbas, W.K. Al-Azzawi, M.M. Hanoon, A.A. Alamiery, W.N.R. Wan Isahak and A.A.H. Kadhum, Corrosion inhibition of mild steel in hydrochloric acid environment using thiadiazole derivative: weight loss, thermodynamics, adsorption and computational investigations, *South Afr J. Chem Eng*., 2022, 41, 244–252. doi: 10.1016/j.sajce.2022.06.011.

6. Z. Yang, L. Shi, M. Zou and C. Wang, Factors influencing the CO2 corrosion pattern of oil–water mixed transmission pipeline during high water content period, *Atmosphere*, 2022, 13, no. 10, 1687. doi: 10.3390/atmos13101687.

7. O.C. Nkuzinna, M.C. Menkiti, O.D. Onukwuli, G.O. Mbah, B.I. Okolo, M.C. Egbujor and R.M. Government, Application of factorial design of experiment for optimization of inhibition effect of acid extract of *gnetum africana* on copper corrosion, *Nat. Resour.,* 2014, 5, no. 7, 299-307. doi: 10.4236/nr.2014.57028.

8. L. Chen, D. Lu and Y. Zhang, Organic compounds as corrosion inhibitors for carbon steel in HCl solution: a comprehensive review, *Materials*, 2022, 15, no. 6, 2023. doi: 10.3390/ma15062023.

ISSN 0795 - 22066

10. M.A. Bedair, H.M. Elaryian, E.S. Gad, M. Alshareef, A.H. Bedair, R.M. Aboushahba and A.E.S Fouda, Insights into the adsorption and corrosion inhibition properties of newly synthesized diazinylderivatives for mild steel in hydrochloric acid: synthesis, electrochemical, SRB biological resistivity and quantum chemical calculations, *RSC Adv*., 2023, 13, 478-498. doi: 10.1039/d2ra06574f.

11. S.N. Dalhatu, K.A. Modu, A.A. Mahmoud, Z.U. Zango, A.B. Umar, F. Usman, J.O. Dennis, A. Alsadig, K.H. Ibnaouf, and O.A. Aldaghri, L-Arginine grafted chitosan as corrosion inhibitor for mild steel protection, *Polymers*, 2023, 15, no. 2, 398. doi: 10.3390/polym15020398.

12. H.E. Aadad, M. Galai, M. Ouakki, A. Elgendy, M.E. Touhami and A. Chahine, Improvement of the corrosion resistance of mild steel in sulfuric acid by new organic-inorganic hybrids of Benzimidazole-Pyrophosphate: Facile synthesis, characterization, experimental and theoretical calculations (DFT and MC). *Surf. Interfaces*., 2021, 24, 101084. doi: 10.1016/j.surfin.2021.101084.

13. A. Zaher, A. Chaouiki, R. Salghi, A. Boukhraz, B. Bourkhiss and M. Ouhssine, Inhibition of mild steel corrosion in 1m hydrochloric medium by the methanolic extract of Ammi visnaga L. Lam seeds, *Int J Corros*., 2020, 2020, no. 1. 1-10. doi: 10.1155/2020/9764206.

14. A. Kadhum, I.N. Betti, A. Al-Adili, L.M. Shaker and A.A. Al-Amiery, Limits and developments in organic inhibitors for corrosion of mild steel: a critical review (Part two: 4-aminoantipyrine). *Int. J. Corros. Scale Inhib*., 2022, 11, no.1, 43–63. doi: 10.17675/2305-6894-2022-11-1-2.

15. N.O. Eddy, S.A. Odoemelam and E. Ibiam (2010). Ethanol extract of Occimium gratissimum as a green corrosion inhibitor for mild steel in H_2SO_4, *Green Chem Lett Rev*., 2010, 3, no.3, 165-172. doi: 10.1080/17518251003636428.

16. N.O. Eddy and S.A. Odoemelam, Inhibition of the corrosion of mild steel in H_2SO_4 by ethanol extract of *Aloe vera. Pigment Resin Technol*., 2009, 38, no.2, 111-115. doi: 10.1108/03699420910940617.

17. E.H. Ali, J.A. Naser, Z.W. Ahmed and T.A. Himdan, Corrosion Protection of 5083 AA in SalineWater by Polyacrylonitrile Nanofibers. *J. Renew. Mater*., 2021, 9, no.11, 1927-1939. doi: 10.32604/jrm.2021.015624.

18. T.D. Manh, T.L. Huynh, B.V. Thi, S. Lee, J. Yi and N.N. Dang, Corrosion inhibition of mild steel in hydrochloric acid environments containing sonneratia caseolaris leaf extract, *ACS Omega*, 2022, 7, no.10, 8874−8886. doi: 10.1021/acsomega.1c07237.

19. S.A. Ajeel, H.M. Waadulah and D.A. Sultan, Effects of H2SO4 and HCl concentration on the corrosion resistance of protected low carbon steel. *Al-Rafidain Eng J*., 2012, 20, no.6, 70-76. doi: 10.33899/rengj.2012.63393.

20. E.C. Benedict, T.O. Chime and E. Osoka, Optimization and effect of leaves extracts on corrosion of mild steal in acidic medium. *Int J Biosci, Biochem Bioinform*., 2020, 10, no.2, 117-126. doi: 10.17706/ijbbb.2020.10.2.117-126.

21. A.Yurt, A. Balaban, S.U. Kandemer, G. Bereket and B. Erk, Investigation of some schiff bases as HCl corrosion inhibitors for carbon steel. *Mater Chem Phys*, 2004, 85, no. 2-3, 420-426. doi: 10.1016/j.matchemphys.2004.01.033.

22. S.K. Saha, M. Murmu, N.C. Murmu and P. Banerjee, Evaluating electronic structure of quinazolinone and pyrimidinone molecules for its corrosion inhibition effectiveness on target specific mild steel in the acidic medium: a combined DFT and MD simulation study. *J Mol Liq*, 2016, 224, 629-638.M doi: 10.1016/j.molliq.2016.09.110.

23. C. Mateos, M.J. Nieves-Remacha and J.A. Rincón, Automated platforms for reaction self-optimization in flow. *React Chem*

ISSN 0795 - 22066

Eng, 2019, 4 no. 9, 1536-1544. doi:10.1039/C9RE00116F.

24. C. Verma, M.A. Quraishi and K. Kluza, Makowska-Janusik M, Olasunkanmi LO, Ebenso EE. Corrosion inhibition of mild steel in 1M HCl by D-glucose derivatives of dihydropyrido [2, 3-d: 6, 5-d 0] dipyrimidine-2, 4, 6, 8 (1H, 3H, 5H, 7H)-tetraone. *Sci. Rep*, 2017, 7, 44432. doi:10.1038/srep44432.

25. N.O. Eddy, H. Momoh-Yahaya and E.E Oguzie, Theoretical and experimental studies on the corrosion inhibition potentials of some purines for aluminum in 0.1 M HCl, *J. Adv. Res*., 2015, 6, no.2, 203-217. doi: 10.1016/j.jare.2014.01.004.

26. B.E. Brycki, I.H. Kowalczyk, A. Szulc, O. Kaczerewska and M. Pakiet. Organic Corrosion Inhibitors, "corrosion inhibitors, Principles and Resent Applications. 2018. doi: 10.5772/intechopen.72943.

37. W. Emori, H. Louis, S.A. Adalikwu, R.A. Timothy, C.R. Cheng, T.E. Gber and A.S. Adeyinka, Molecular modeling of the spectroscopic, structural, and bioactive potential of tetrahydropalmatine: insight from experimental and theoretical approach, *Polycycl Aromat Compd*, 2022, 2022, 1-18. doi:10.1080/10406638.2022.2110908E.

38. A. Eno, C.R. Cheng, H. Louis, T.E. Gber, W. Emori, I.A.T. Ita and A.S. Adeyinka, Investigation on the molecular, electronic and spectroscopic properties of rosmarinic acid: an intuition from an experimental and computational perspective, *J Biomol Struct Dyn*, 2022, 22:1-15. doi: 10.1080/07391102.2022.2154841.

39. S. Erdoğan, Z.S. Safi, S. Kaya, D.O Işın, L. Guo and C. Kaya, A computational study on corrosion inhibition performances of novel quinoline derivatives against the corrosion of iron, *J Mol Struct*, 2017, 1134, 751-761. doi: 10.1016/j.molstruc.2017.01.037.

40. J.A. Agwupuye, T.E. Gber, H.O. Edet, M. Zeeshan, S. Batool, O.E. Duke and G.E. Egbung, Molecular Modeling, DFT studies and Biological Evaluation of methyl 2, 8-dichloro-1, 2-dihydroquinoline-3-carboxylate. *Chem Phys Impact*, 2022, 6, 100146. doi: 10.1016/j.chphi.2022.100146.

41. H. Kumar and T. Dhanda, Cyclohexylamine an effective corrosion inhibitor for mild steel in 0.1 N H2SO4: Experimental and theoretical (molecular dynamics simulation and FMO) study, *J Mol Liq*, 2021, 327, 114847. doi: 10.1016/j.molliq.2020.114847.

42. I. B. Obot, Z. M. Gasem and S. A. Umoren, Molecular-level understanding of the mechanism of aloes leaves extract inhibition of low carbon steel corrosion: a DFT approach, *Int. J. Electrochem. Sci*, 2014, 9, no. 2, 510 – 522

43. I. Benjamin, T.E. Gber, H. Louis, T.N. Ntui, E.I, Oyo-Ita, T.O. Unimuke and A.S. Adeyinka, Modelling of aminothiophene-carbonitrile derivatives as potential drug candidates for hepatitis B and C, *Iran J Sci Technol, Transact A: Sci,* 2022, 46 no.5, 1399-1412. doi:10.1007/s40995-022-01355-w

44. C.G. Apebende, P.S. Idante, H. Louis, U.S Ameuru, T.O. Unimuke, T.E. Gber and F.C. Asogwa, Integrated spectroscopic, bio-active prediction and analytics of isoquinoline derivative for breast cancer mitigation. *Chem Afri*, 2022, 5 no.6, 1979-1995. doi:10.1007/s42250-022-00479-1

45. S. Aayisha, T.R. Devi, S. Janani, S. Muthu, M. Raja and S. Sevvanthi, DFT, molecular docking and experimental FT-IR, FT-Raman, NMR inquisitions on "4-chloro-N-(4, 5-dihydro-1H-imidazol-2-yl)-6-methoxy-2-methylpyrimidin-5-amine": alpha-2-imidazoline receptor agonist antihypertensive agent. *J Mol Struct*, 2019, 1186, 468-481. doi: 10.1016/j.molstruc.2019.03.056

46. J.P. Nascimento, J.R.A. Silva, J. Lameira and C.N. Alves, Metal-dependent inhibition of HIV-1 integrase by 5CITEP inhibitor: a theoretical QM/MM approach. *Chem Phys Lett*, 2013, 583, 175-179. /doi: 10.1016/j.cplett.2013.08.006

ISSN 0795 - 22066

47. R. Dennington, T.A. Keith and J.M. Millam, GaussView 6.0. 16. Semichem Inc.: Shawnee Mission, KS, USA 2016.

48. S. Moro, M. Bacilieri, C. Ferrari, G. Spalluto, Autocorrelation of molecular electrostatic potential surface properties combined with partial least squares analysis as alternative attractive tool to generate ligand-based 3D-QSARs. *Curr Drug Discov Tech*, 2005, 2 no. 1, 13-21. doi: 10.2174/1570163053175439.

49. B.A. Farzana, A.M. Banu and K.R. Ahamed, K. R. Andrographis echioides leaves extract as an eco-friendly corrosion inhibitor for mild steel in acid medium. *Mater Today: Proceed*, 2021, 47, 2080-2090. doi.org/10.1016/j.matpr.2021.04.478

50. M.E. Belghiti, S. Echihi, A. Dafali, Y. Karzazi, M. Bakasse, H. Elalaoui-Elabdallaoui and M. Tabyaoui, Computational simulation and statistical analysis on the relationship between corrosion inhibition efficiency and molecular structure of some hydrazine derivatives in phosphoric acid on mild steel surface. *Appl Surf Sci*, 2019, 491, 707-722. doi: 10.1016/j.apsusc.2019.04.125.

ISSN 0795 - 22066